



Simulation guided design of the MRcollar: a MR compatible applicator for deep heating in the head and neck region

Tomas Drizdal, Kemal Sumser, Gennaro G. Bellizzi, Ondrej Fiser, Jan Vrba, Gerard C. van Rhoon, Desmond T. B. Yeo & Margarethus M. Paulides

To cite this article: Tomas Drizdal, Kemal Sumser, Gennaro G. Bellizzi, Ondrej Fiser, Jan Vrba, Gerard C. van Rhoon, Desmond T. B. Yeo & Margarethus M. Paulides (2021) Simulation guided design of the MRcollar: a MR compatible applicator for deep heating in the head and neck region, International Journal of Hyperthermia, 38:1, 382-392, DOI: [10.1080/02656736.2021.1892836](https://doi.org/10.1080/02656736.2021.1892836)

To link to this article: <https://doi.org/10.1080/02656736.2021.1892836>



© 2021 The Author(s). Published with license by Taylor & Francis Group, LLC



Published online: 07 Mar 2021.



[Submit your article to this journal](#)



Article views: 1524



[View related articles](#)



[View Crossmark data](#)



Citing articles: 2 [View citing articles](#)

Simulation guided design of the MRcollar: a MR compatible applicator for deep heating in the head and neck region

Tomas Drizdal^{a,b} , Kemal Sumser^a , Gennaro G. Bellizzi^{a,c} , Ondrej Fiser^b , Jan Vrba^b , Gerard C. van Rhooon^a , Desmond T. B. Yeo^d  and Margarethus M. Paulides^{a,e} 

^aHyperthermia Unit, Department of Radiotherapy, Erasmus MC Cancer Institute, Rotterdam, The Netherlands; ^bDepartment of Biomedical Technology, Faculty of Biomedical Engineering, Czech Technical University in Prague, Kladno, Czech Republic; ^cDepartment of Information Engineering, Infrastructures and Sustainable Energy, Università Mediterranea di Reggio Calabria, Reggio di Calabria, Italy; ^dImaging and Bioelectronic Technologies, GE Global Research Centre, Niskayuna, NY, USA; ^eDepartment of Electrical Engineering, Eindhoven University of Technology, Eindhoven, The Netherlands

ABSTRACT

Purpose: To develop a head and neck hyperthermia phased array system compatible with a 1.5 T magnetic resonance (MR) scanner for noninvasive thermometry.

Methods: We designed a dielectric-parabolic-reflector antenna (DiPRA) based on a printed reflector backed dipole antenna and studied its predicted and measured performance in a flat configuration (30 mm thick water bolus and muscle equivalent layer). Thereafter, we designed a phased array applicator model ('MRcollar') consisting of 12 DiPRA modules placed on a radius of 180 mm. Theoretical heating performance of the MRcollar model was benchmarked against the current clinical applicator (HYPERcollar3D) using specific (3D) head and neck models of 28 treated patients. Lastly, we assessed the influence of the DiPRA modules on MR scanning quality.

Results: The predicted and measured reflection coefficients (S_{11}) of the DiPRA module are below -20 dB. The maximum specific absorption rate (SAR) in the area under the antenna was 47% higher than for the antenna without encasing. Compared to the HYPERcollar3D, the MRcollar design incorporates 31% less demineralized water (-2.5 L), improves the predicted TC25 (target volume enclosed by 25% iso-SAR contour) by 4.1% and TC50 by 8.5%, while the target-to-hotspot quotient (THQ) is minimally affected (-1.6%). MR experiments showed that the DiPRA modules do not affect MR transmit/receive performance.

Conclusion: Our results suggest that head and neck hyperthermia delivery quality with the MRcollar can be maintained, while facilitating simultaneous noninvasive MR thermometry for treatment monitoring and control.

ARTICLE HISTORY

Received 5 June 2020
Revised 4 February 2021
Accepted 15 February 2021

KEYWORDS



Antenna; phased array; head and neck; SAR; magnetic resonance

Introduction

Hyperthermia has proven beneficial when added to standard radiotherapy and chemotherapy for treatment of many tumor locations, including the head and neck (H&N) [1–4]. In order to elevate the temperature in the H&N region to the desired range of 40–44 °C, we have previously developed the unique HYPERcollar3D applicator consisting of 20 patch antennas operating at 434 MHz [5,6]. At Erasmus MC, hyperthermia using the HYPERcollar3D is being applied once a week for 75 min after the radiotherapy treatment [7]. The temperature during the hyperthermia is measured superficially and, whenever possible, interstitially by sets of fiber optic probe sensors placed in closed tip catheters. Magnetic resonance (MR) imaging has shown to have a clinical potential for noninvasive temperature measurement in the pelvic region, however no device exists for MR-hyperthermia in the

H&N [8,9]. In 2012, we therefore started to study the feasibility of integrating the hyperthermia H&N device into an MR scanner for noninvasive MR thermometry by developing a novel applicator: the MRcollar.

Integrating a hyperthermia system into the MR requires the use of nonmagnetic components and design principles that minimize system-induced image artifacts. One example for this is the minimization of large electrically conductive surfaces that can generate undesired gradient-induced eddy-currents or shield certain regions of interest from the MR radiofrequency (RF) transmit fields. Previously, we redesigned the HYPERcollar3D and experimentally showed the feasibility of applying hyperthermia in a 1.5 T GE 450w MR scanner using the 'MRlabcollar', a laboratory prototype consisting of 12 patch antennas operating at 434 MHz [10–12]. In those measurements, we observed that the connectors of the antennas caused image distortion in the MR thermometry

CONTACT Tomas Drizdal  t.drizdal@erasmusmc.nl  Hyperthermia Unit, Department of Radiotherapy Erasmus MC Cancer Institute, Dr. Molewaterplein, Rotterdam, 3015 GD Rotterdam, The Netherlands

This article has been republished with minor changes. These changes do not impact the academic content of the article

© 2021 The Author(s). Published with license by Taylor & Francis Group, LLC

This is an Open Access article distributed under the terms of the Creative Commons Attribution License (<http://creativecommons.org/licenses/by/4.0/>), which permits unrestricted use, distribution, and reproduction in any medium, provided the original work is properly cited.

images, even if the effects were located on the periphery of the water bolus structure and not within the region of interest. Motivated by the negligible MR distortions found for the self-grounded bow-tie antenna, we developed the Yagi-Uda antenna, which has a smaller cross-section of metal obstructing the B_1^+ field [13–15].

Noninvasive MR thermometry using the MR scanner is clinically available for deep hyperthermia in the pelvic region using the Sigma Eye system (Pyrexar Medical, Salt Lake City, USA) [16,17]. Sigma Eye and MRlabcollar use independent systems for MR thermometry and hyperthermia heating. This differs from other approaches where the hyperthermia and MR imaging functionalities are embedded into a common antenna structure. It was demonstrated that a 3T MR surface loop coil array can be modified in real time into a C-shaped dipole antenna phased array for hyperthermia heating using fast RF switches [18,19]. As an alternative, Winter et al. proposed to use a bow-tie antenna system for imaging and heating at 7T (298.6 MHz) [20,21]. Both these approaches use the MR scanner RF amplifiers for heating and thus don't allow truly simultaneous heating and imaging. Further they also restrict the heating frequency to the Larmor frequency, which is often not the optimum choice considering focusing and operational costs. Hence, the optimum choice might be an appropriate co-design of a heating antenna array and imaging coil arrays. We selected 434 MHz as operating frequency as it is within the band of optimum frequencies [22] and an ISM (industrial, scientific and medical) frequency for which low-cost amplifiers are available. This frequency is also sufficiently far from the Larmor frequency (64 MHz) and higher order modes of a 1.5T MR scanner, which enables decoupled operation for truly simultaneous noninvasive MR thermometry [9].

The purpose of this study was to use 3D electromagnetic (EM) field modeling to design a clinical applicator prototype for MR guided deep hyperthermia treatment in the H&N region. In the first step, we designed the dielectric parabolic reflector antenna (DiPRA) module. In the second step, we used a dedicated measurement setup to verify the predicted reflection coefficient and radiation characteristic of the DiPRA module. Based on this module, we then created a phased array applicator (MRcollar) model and tailored its dimensions to the average H&N patient. Forth, the predicted heating capabilities of the MRcollar design were evaluated against the clinically used HYPERcollar3D applicator [23]. Finally, MR experiments were carried out to assess the influence of the DiPRA modules on MR scanning quality.

Methods

Antenna encasing – DiPRA module

Figure 1(a) shows the original Yagi-Uda antenna model in Sim4Life (v. 4.4, Zürich MedTech AG, Zürich, Switzerland), for which heating performance and MR compatibility were verified in a previous study [13]. The antenna was manufactured at an FR-4 printed circuit board and operates at 434 MHz. It is partly submerged in the de-mineralized water bolus, which allows reducing the antenna size, efficient EM energy transfer and cooling of the patient surface. The director of the

printed circuit board (PCB) Yagi-Uda antenna (Figure 1(a)) was removed to reduce axial size and because it induced significant sensitivity in impedance characteristics to the cavity enclosing. This removal resulted in a reflector backed dipole antenna shown in Figure 1(b). To reduce the amount of water needed, minimize the cross-coupling and improve focusing, we designed a specific encasing with a parabolic back shape shown in Figure 1(c), a dielectric parabolic reflector antenna (DiPRA). The width of the DiPRA encasing (w_e), shown in Figure 1(c), is determined by the 70 mm printed reflector backed dipole antenna width. The height (h_e) was selected such that the specific absorption rate (SAR) in the muscle equivalent phantom was not influenced by this dimension. The distance between antenna and cavity top (d_{a-e}) and the thickness of the top encasing part (d_{et}), shown in Figure 1(d), were selected to have a minimum influence on the antenna reflection characteristics. We placed the DiPRA module on a $30 \times 300 \times 300 \text{ mm}^3$ water bolus and a $100 \times 300 \times 300 \text{ mm}^3$ muscle equivalent phantom model, and studied reflection coefficient and SAR characteristics. For the FR-4 substrate we applied $\epsilon_r = 4.66$, $\sigma = 1.9 \text{ mS/m}$, $\rho = 1850 \text{ kg/m}^3$ dielectric properties, for the antenna encasings $\epsilon_r = 2.6$, $\sigma = 4 \text{ mS/m}$, $\rho = 1180 \text{ kg/m}^3$, for the water bolus $\epsilon_r = 80$, $\sigma = 0.04 \text{ S/m}$, $\rho = 1000 \text{ kg/m}^3$ and for the phantom $\epsilon_r = 56.9$, $\sigma = 0.81 \text{ S/m}$, $\rho = 1090 \text{ kg/m}^3$.

DiPRA module verification measurements

To validate this embedded antenna concept, we created a dedicated measurement setup in Sim4Life, as shown in Figure 2(a). Figure 2(b) shows the manufactured setup using polyethylene terephthalate glycol (PET-G) filament printed with 0.4 mm nozzle diameter, 0.25 mm layer height and 100% filling factor at Prusa i3 MK3 (Prusa Research, Prague, Czech Republic) 3D printer. A two-component epoxide glue (Chemex POX Z 21, Prague, Czech Republic) was applied for antenna fixation and coating of the 3D printed part ensuring water resistance of the entire measurement setup. We also 3D printed a 30 mm height frame for the water bolus filled with demineralized water. For the reflection coefficient measurements, we created a phantom with muscle equivalent properties at 434 MHz consisting of demineralized water, salt and isopropyl alcohol. The concentrations of the individual components were adjusted in a few iterative steps using dielectric assessment kit DAK-12 (SPEAG, Zürich, Switzerland) connected to N9923A FieldFox vector network analyzer (Keysight, Santa Rosa, USA). This procedure resulted in a liquid phantom with a relative permittivity of $\epsilon_r = 56.4$ and an electric conductivity of $\sigma = 0.79 \text{ S/m}$. These values were very close to the literature values for muscle of $\epsilon_r = 56.9$ and $\sigma = 0.81 \text{ S/m}$ used for the hyperthermia treatment planning purposes within this study. The reflection coefficient characteristics were measured for different encasing top thicknesses, ranging from 0.5 mm to 1.5 mm, using a liquid phantom and a FSH8 (Rohde&Schwarz, Munich, Germany) vector network analyzer.

For the SAR measurements, we prepared a solid phantom following the procedure recommended for superficial

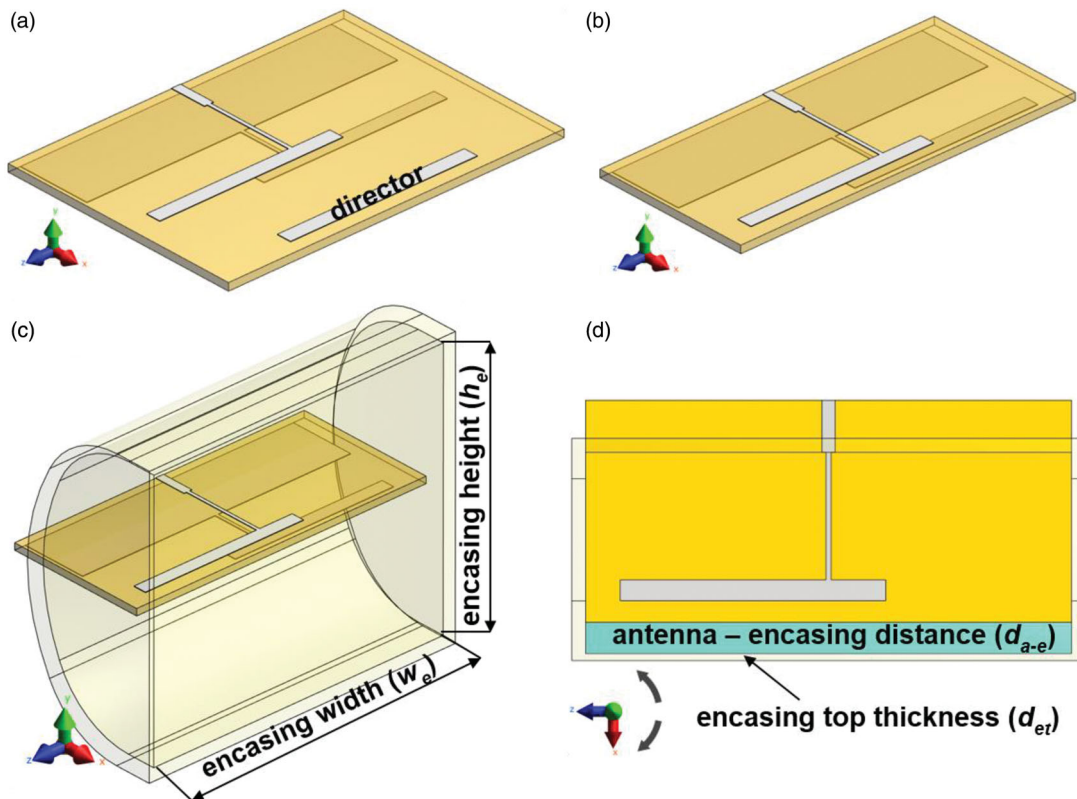


Figure 1. Models of (a) original Yagi-Uda antenna including director, (b) reflector backed dipole antenna, (c) dielectric parabolic reflector antenna (DiPRA) module, (d) 2D planar cross-section of the DiPRA module.

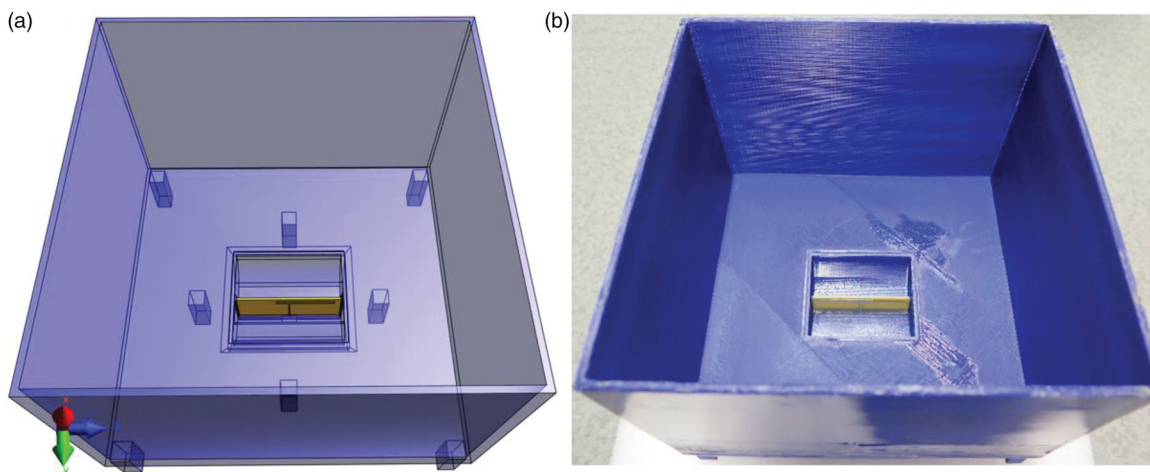


Figure 2. (a) model of DiPRA verification setup (note that the 3D printed part model is transparent and perspective view is used for better clarity), (b) manufactured setup using 3D printer technology.

hyperthermia quality assurance [24]. The phantom consisted of demineralized water, salt, agar powder, TX-151 and polyethylene powder and its dielectric properties ($\epsilon_r=66$, $\sigma=0.925/\text{m}$) were measured using DAK-12. The phantom was filled in eight 10 mm 3D printed frames which were placed on the top of another inside the 3D printed container. After heating period, the whole phantom was taken out from the container and two 2D profiles in depth of 12.8 mm and 24.5 mm depths measured by removing top phantom layers. These thicknesses correspond to the manually measured thicknesses of the first and second phantom layers after phantom creation. The SAR characteristics were

measured using E60 FLIR (FLIR Systems, Wilsonville, USA) for the scenario without antenna encasing cover and for the scenario with a 1 mm thick cover. The 75 W harmonic signal at 434 MHz was excited using a PG 70.150.2 (SSB Electronics GmbH, Lippstadt, Germany) power generator and guided via a ZGBDC30-372HP+ (MiniCircuits, Brooklyn, USA) bi-directional coupler toward the DiPRA panel SMA type connector. Forward and reflected power were acquired using two PWR-6GHZ (MiniCircuits, Brooklyn, USA) power meters connected with 20 dB additional attenuation to the outputs of the bidirectional coupler. Its attenuation and coupling characteristics were measured at the beginning of the experiments with a

FSH8 vector network analyzer. We calculated SAR using the specific heat capacity ($c = 3640 \text{ J/kg/K}$) multiplied by the empirical rate of temperature rise. The latter is computed from the ratio of measured temperature increase (subtracted 2D infrared images after and before the heating) and the measurement time (four minutes). SAR was normalized to 1 W input power to enable comparison of predicted and measured SAR distributions. The predicted 2D SAR profiles were extracted at corresponding depths from homogenous phantom model.

MRcollar design

Figure 3(a) shows the simulation setup of the MRcollar model consisting of 12 antennas organized in two 2×3 DiPRA arrays applied from left and right side of the patient H&N model. Distances between individual DiPRA modules and the patient surface characterize the water bolus thickness. To provide more evenly distributed water bolus pressure to the patient and a more homogenous water circulation throughout the water bolus, it is desirable to keep the water bolus thickness constant for the whole MRcollar model. We approximated the surface of the representative patient with a radius of curvature of 150 mm, to which we added 30 mm of water bolus thickness. This resulted in the final 180 mm radius of the both 2×3 arrays parts of the MRcollar model shown in Figure 3(b). A rounding with a radius of 180 mm was applied to the footprint of the antenna modules in order to provide better contact between water bolus and the modules.

MRcollar model heating capabilities

Heating capabilities of the clinically used HYPERcollar3D and the MRcollar model were evaluated on data from 28 H&N patients for which hyperthermia treatment planning (HTP) was previously done. The patient group consisted of 14 oropharynx, five neck node, three nasopharynx, three larynx, two oral cavity and one hypopharynx tumors, i.e., 19 males and nine females with a mean age of 63.1 ± 11.2 years. Patient specific 3D H&N models were created from computed tomography (CT) images using an atlas based automatic segmentation routine followed, if necessary, by manual adjustments in iSeg (v. 3.8, Zürich MedTech AG, Zürich, Switzerland) [25]. Then the patient models were imported into Sim4Life, together with the HYPERcollar3D or the MRcollar model, for EM field simulations. All dielectric properties were assigned from the IT'IS database available in Sim4Life at 434 MHz [26]. For the HYPERcollar3D models, we used 1.5 mm global finite difference time domain (FDTD) grid step refined to 1.25 mm within the HYPERcollar3D model and to 0.75 mm for the patch antenna parts. For the MRcollar models, we used 1.5 mm global FDTD grid step refined to 1 mm for the antenna encasing, 0.75 mm for the metallic antenna parts and 0.5 mm at the discrete edge source feeding. Typical size of the whole FDTD calculation domain for both models was around 90 million cells. A 434 MHz excitation and 20 periods of harmonic signal were

applied for each antenna. We used computed unified device architecture (CUDA) acceleration at nVidia GTX 1080 Ti graphical processor units resulting in a typical computation time for each simulation of 35 min for the MRcollar model and 15 min for the HYPERcollar3D model.

Afterwards, all simulations were exported to VEDO, our in-house developed visualization tool for electromagnetic dosimetry and optimization [27]. VEDO allows pretreatment and online optimization of the amplitude and phase feeding signals of individual antennas in order to maximize the EM field energy focus in the target region. It uses the particle swarm optimization toolbox to optimize target-to-hotspot quotient (THQ) representing a ratio between the average SAR in the target and the average SAR in the hotspot (total volume with the highest 1% SAR outside the target) [28,29]. In addition to THQ, we also compared the target volume coverage of the 25% and 50% SAR iso-contour, TC25 and TC50.

MR assessment of antenna encasing – DiPRA module

We investigated the influence of the DiPRA module on MR quality following the tests recommended in Hoffmann et al. [30]. Three comparative tests were used to assess the absence of field distortions on B_0 and B_1^+ as well as SNR performance, respectively. Although DiPRA modules are not intended to be used as MR transmit or receive coils for which the guidelines in Hoffmann are designed, these tests are relevant to investigate possible MR distortions caused by the DiPRA modules. In that regard, both one and two DiPRA modules scenarios were tested. In the experimental setup, the DiPRA modules were placed on top of a static water bolus that was positioned in turn on top of a calibration phantom provided by the MR vendor (GE Medical Systems - MR Division, Waukesha, WI, CTL Lower TL, P/N U1150027: $T_1 = 108 \text{ ms}$; $T_2 = 96 \text{ ms}$). Both B_0 field and flip angle distortions were assessed by comparing the homogeneity in a single slice when the DiPRA modules are present to the homogeneity when they are absent. B_0 field homogeneity was measured with a dual echo gradient echo sequence [31] (slice thickness 2.9 mm, FOV $300 \times 300 \text{ mm}^2$, matrix 256×256 , TR/TE1/TE2 243/4.6/9.2 ms, NEX 1, flip angle 15°). The flip angle field map was measured using the Bloch-Siegert method [32] (slice thickness 5 mm, FOV $300 \times 300 \text{ mm}^2$, matrix 128×128 , TR/TE 20/14 ms, NEX 1, flip angle 30°). SNR was measured using a spoiled gradient echo sequence (slice thickness 2 mm, single slice, FOV $300 \times 300 \text{ mm}^2$, matrix 256×256 , TR/TE 75/4.5 ms, NEX 1, flip angle 60°). In order to evaluate the homogeneity of the different fields and compare them, a central region of interest (ROI) was defined, 30 mm deep in the phantom.

Results

Antenna encasing - DiPRA module

Figure 4(a) shows the influence of the distance between the antenna and the encasing cover d_{a-e} (mm) on the antenna reflection coefficient, with the minimum $S_{11} = -44.6 \text{ dB}$

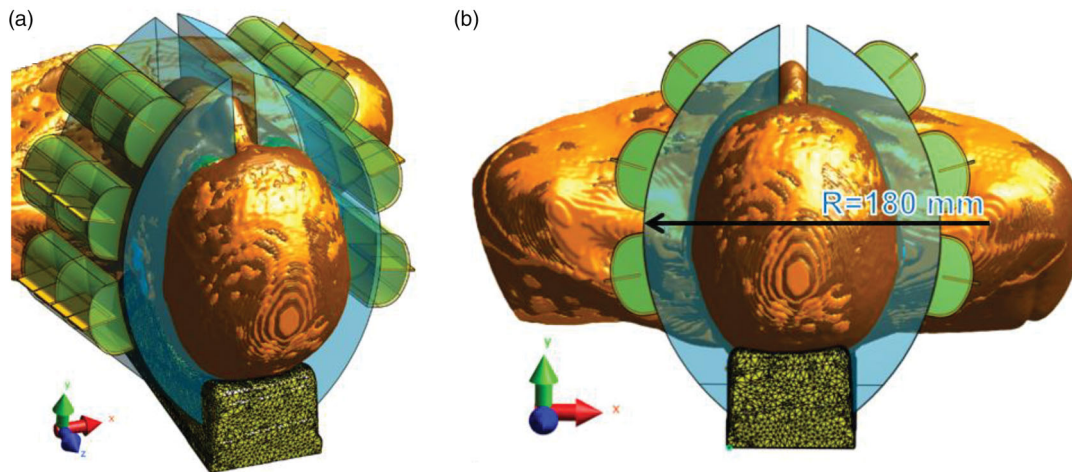


Figure 3. (a) MRcollar model in Sim4Life, (b) MRcollar model with highlighted radius $R = 180$ mm.

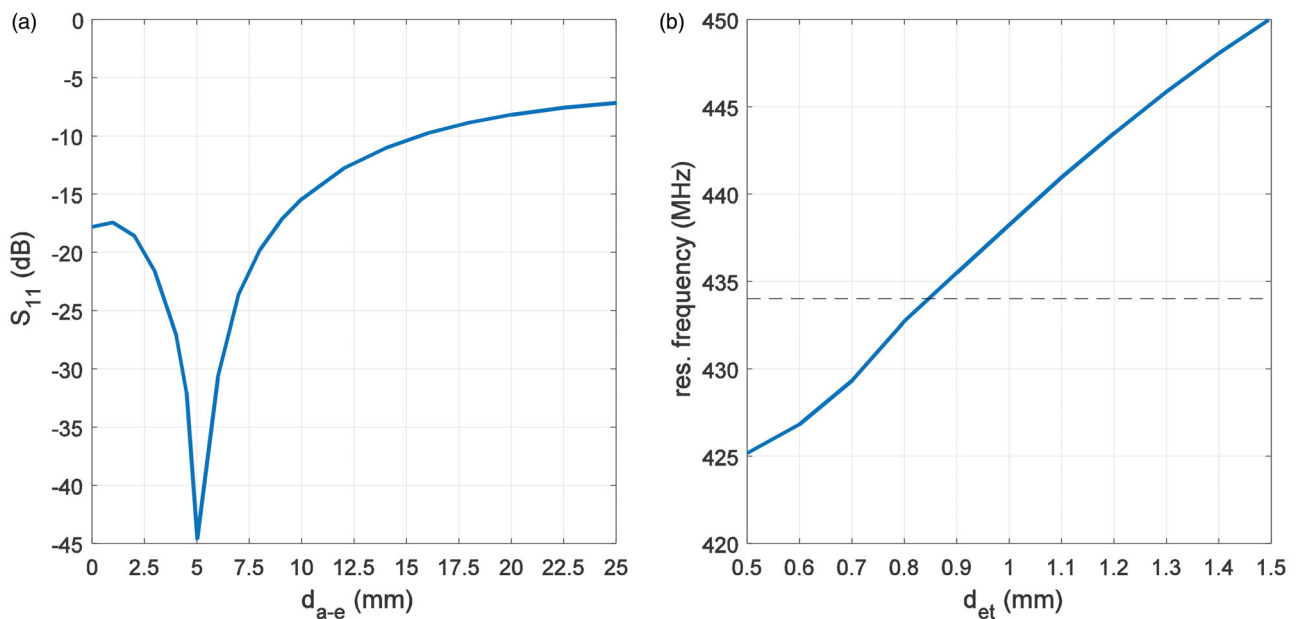


Figure 4. (a) Reflection coefficient (S_{11}) as a function of antenna to antenna top encasing distance d_{a-e} (mm) for $d_{et}=1$ mm, (b) antenna resonant frequency change for various thicknesses of the top encasing d_{et} (mm) for $d_{a-e}=4.5$ mm.

obtained for a distance of 5 mm. We selected $d_{a-e}=4.5$ mm, to account for a larger distance in the curved antenna encasing, ensuring good matching ($S_{11} = -32$ dB). Figure 4(b) illustrates the linear relationship between the top encasing thickness d_{et} (mm) and antenna resonant frequency, calculated for $d_{a-e} = 4.5$ mm. Even though the optimum thickness for resonance at 434 MHz is $d_{et} = 0.85$ mm, we selected $d_{et} = 1$ mm to ensure mechanical and waterproof stability of the antenna encasing.

Figure 5(a) shows the normalized SAR depth profiles for the reflector backed dipole antenna placed in: (1) a flat (brick-shaped) volume of deionized water, (2) encasing without the cover and (3) in full encasing, i.e., the DiPRA. In Figure 5(a), penetration depths equal to 20 mm are observed for the flat water model, as are penetration depths of 21 mm for both scenarios with encasing. These values were calculated following the single antenna guidelines of ESHO [24]. When introducing the encasing around the reflector backed dipole antenna, the maximum SAR increased by 47% in a

muscle equivalent phantom, from 3.4 W/kg to 5 W/kg for 1 W input power. The normalized 2D SAR distribution at 10 mm depth for the DiPRA module in the phantom is shown in Figure 5(b). Figure 5(c,d) show the normalized SAR profiles at 10 mm depth for all three studied scenarios along Y axis and Z axis, respectively. The encasing without the aperture cover had the best SAR symmetry from all three studied scenarios at 10 mm depth of the phantom. A 6 mm maximum SAR shift in -Y direction was observed for the DiPRA module.

DiPRA module verification measurements

Figure 6(a) shows the reflection coefficient comparison for the prediction and two measurements of the DiPRA. For all cases, S_{11} is below -20 dB, which represents maximum reflection of 1% from the input power. Figure 6(b) shows measured DiPRA resonant frequency as a function of top encasing thickness d_{et} (mm).

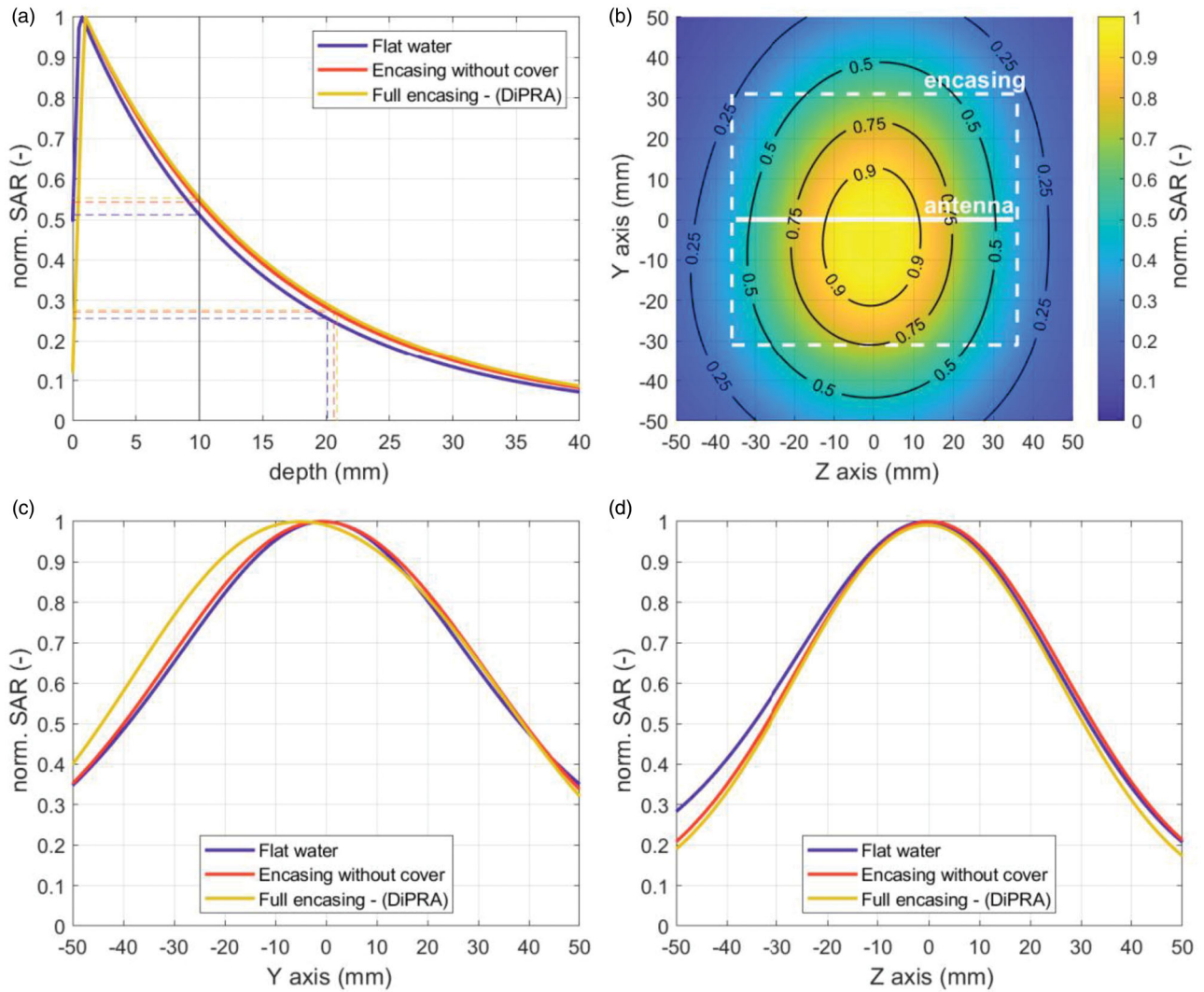


Figure 5. (a) normalized SAR depth profiles for reflector backed dipole antenna module in deionized water, in encasing without the cover part, and in full encasing, i.e., the DiPRA module, (b) normalized 2D SAR profile at 10 mm depth of muscle equivalent phantom for the DiPRA module, highlighted in the figure using solid and dashed lines, (c), (d) normalized SAR profiles at 10 mm depth in the center along Y axis ($Z=0$ mm) and Z axis ($Y=0$ mm), respectively.

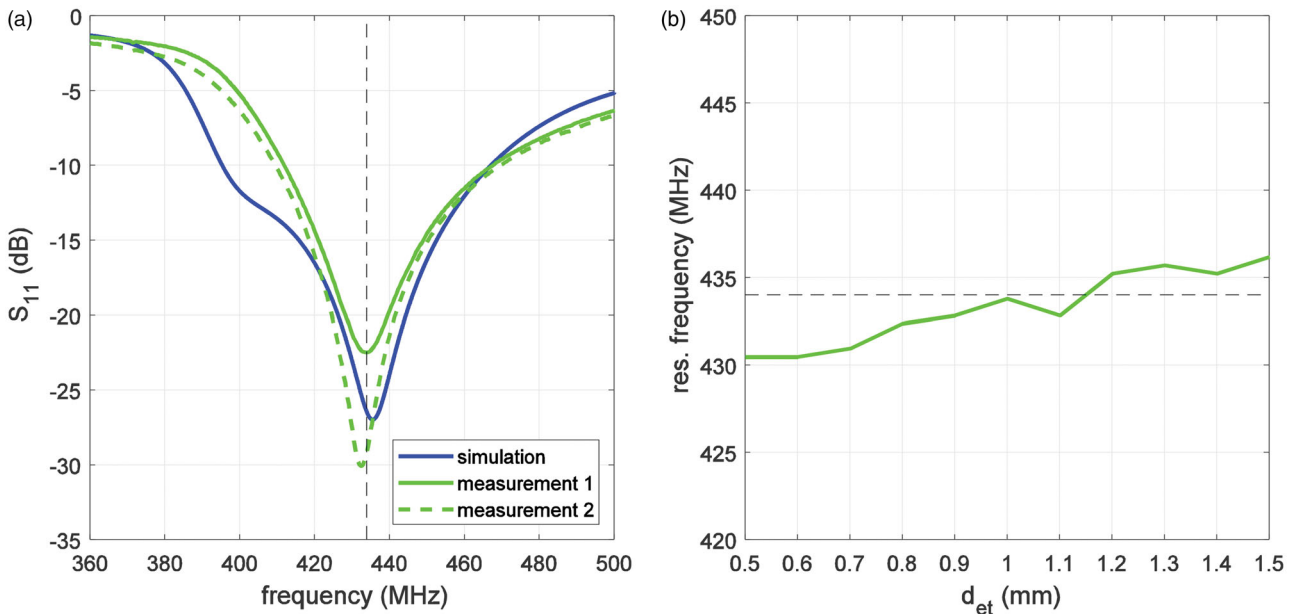


Figure 6. (a) comparison of predicted and measured reflection coefficient for DiPRA with $d_{et}=1$ mm and $d_{a-e}=4.5$ mm, (b) measured DiPRA resonant frequency change versus thickness of the top encasing d_{et} (mm).

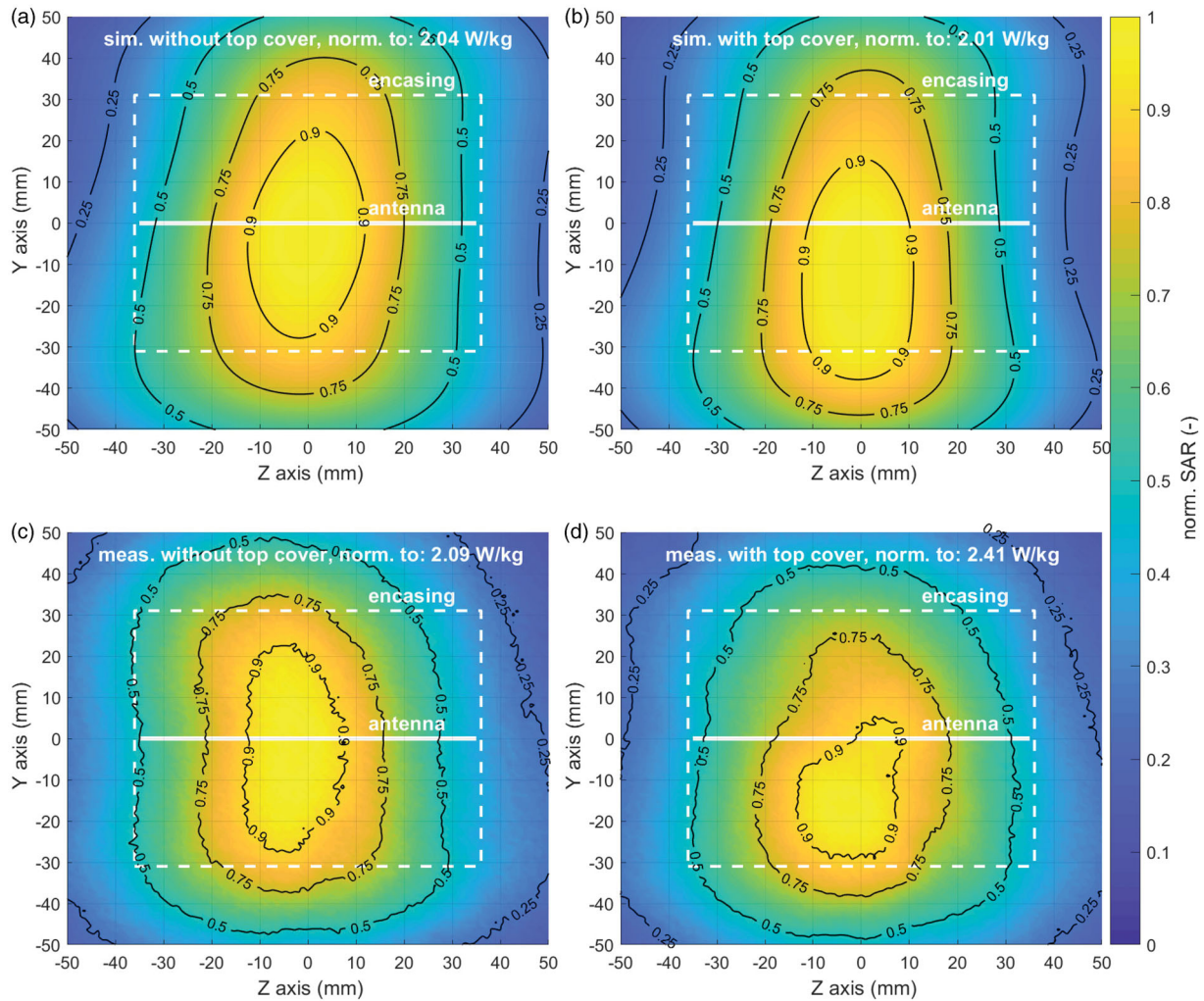


Figure 7. Normalized SAR predictions for DiPRA module (a) without and (b) with top cover, measurements (c) without and (d) with top cover at 12.8 mm phantom depth.

Normalized 1 g SAR predictions and verification measurements for the DiPRA module without and with the 1 mm top cover are shown in [Figure 7\(a,b\)](#) (with) and [Figure 7\(c,d\)](#) (with). The distributions were normalized to the maximum SAR in the 2D plane at 12.8 mm phantom depth, i.e., the height of the first 3D printed frame filled with the agar phantom. For the DiPRA scenario without the top cover, we obtained comparable predicted (2.04 W/kg) and measured (2.09 W/kg) maximum SAR. For the scenario including a 1 mm top cover, the measured maximum SAR (2.41 W/kg) was higher than predicted (2.01 W/kg). In this case, measurement ([Figure 7\(d\)](#)) confirmed the predicted SAR shift when adding 1 mm top cover. [Figure 8](#) shows the corresponding normalized SAR figures at 24.5 mm depth in the agar phantom. At this depth, predicted SAR is higher than measured SAR for both studied DiPRA scenarios.

MRcollar design

For 28 simulation setups we obtained a mean water bolus volume for the HYPERcollar3D of 8.0 ± 0.3 L and 5.5 ± 0.3 L for the MRcollar design. For 22 adjacent DiPRA modules inside the array and all 28 HTP setups, we obtained a cross-

coupling of -23.6 ± 5.1 dB. The maximum cross-coupling of -14.9 dB was observed for the two adjacent modules in the top left corner of the 2×3 array.

MRcollar model heating capabilities

[Figure 9](#) shows the THQ for the MRcollar against the HYPERcollar3D model for 28 H&N patients. For the HYPERcollar3D a mean THQ = 1.25 ± 0.39 was obtained, and 1.23 ± 0.3 was the mean THQ for the MRcollar model, demonstrating comparable heating capabilities of both systems. [Figure 10\(a,b\)](#) show the comparison of target coverage in terms of TC25 and TC50. Higher mean values for the MRcollar model of TC25 = $87.8 \pm 13\%$ and TC50 = $55.5 \pm 23.8\%$ in comparison to TC25 = $83.7 \pm 15.6\%$ and TC50 = $47 \pm 22.1\%$ obtained for the HYPERcollar3D demonstrate improved target coverage for the MRcollar design.

MR assessment of antenna encasing - DiPRA module

[Figure 11](#) shows the results for the magnitude images, the B_0 and flip angle (B_1^+) field maps in absence and presence of the DiPRA modules. The B_0 homogeneity in the absence

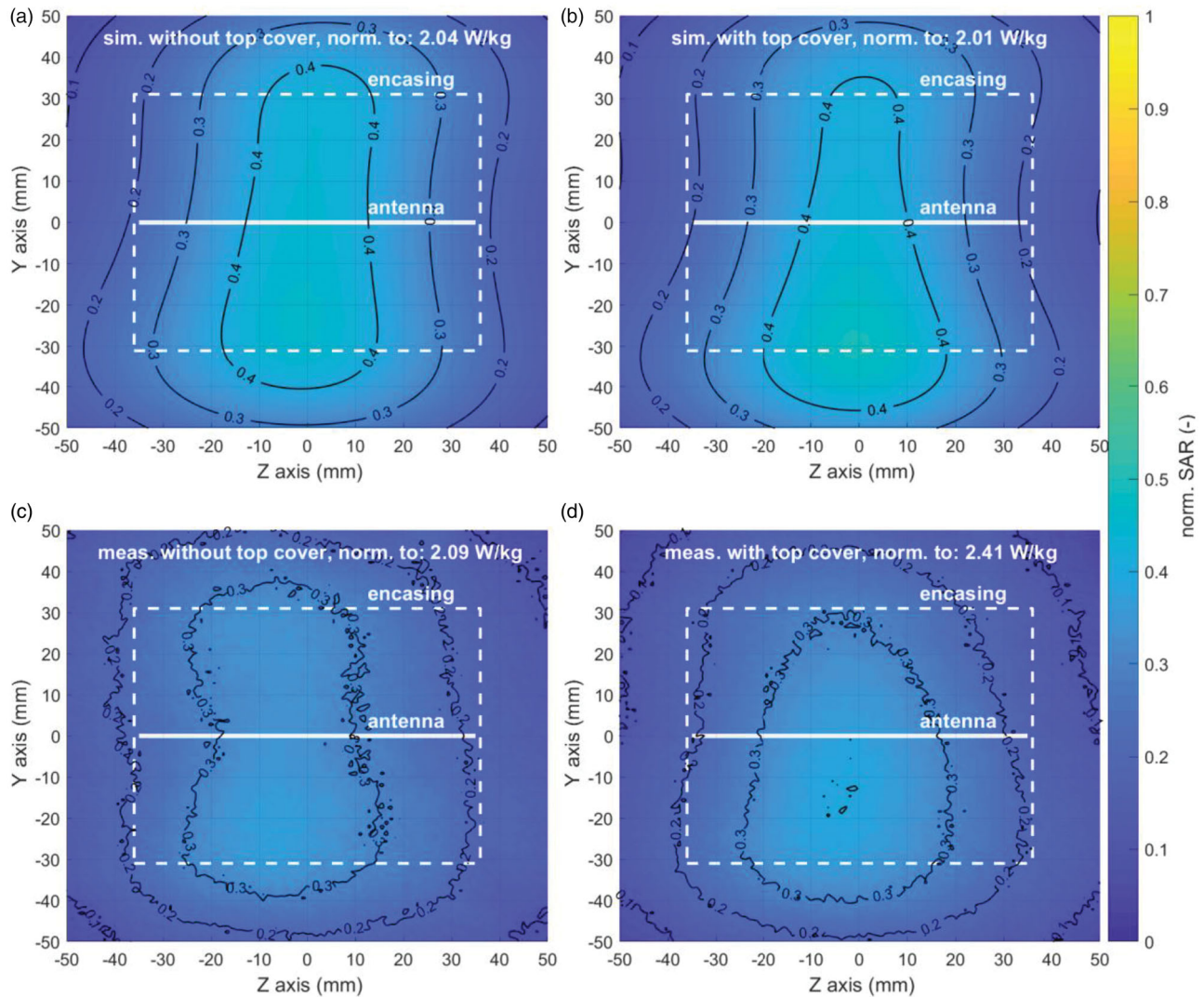


Figure 8. Normalized SAR predictions for DiPRA module (a) without and (b) with 1 mm top cover, measurements (c) without and (d) with top cover at 24.5 mm phantom depth.

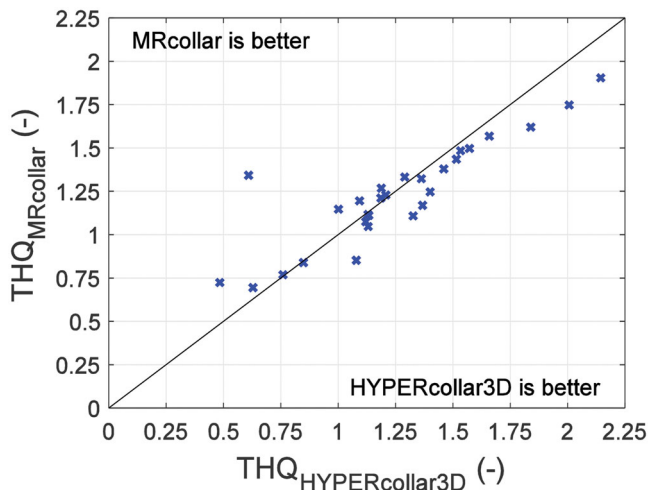


Figure 9. THQ comparison for the MRcollar and the HYPERcollar3D models for 28 H&N patients.

of DiPRA modules had a standard deviation of 8.3 Hz within the ROI. The presence of two DiPRA modules improved B_0 field homogeneity (standard deviation = 7.9 Hz). The mean

flip angle within the ROI was always $32.5 \pm 1.3^\circ$ and hence independent of the presence of DiPRA modules. Finally, the image SNR in the ROI was 156 dB, when no DiPRA modules were present, while the image SNR was slightly higher when one or two DiPRA's were present (163 dB). Overall, a negligible impact on B_0 homogeneity, average flip angle and SNR were observed.

Discussion

The MRcollar design improves the predicted SAR target coverage (TC25 = +4.1% and TC50 = +8.5%) and achieves a comparable target-to-hotspot quotient (THQ = -1.6%) when comparing it to our clinically used HYPERcollar3D system. These improvements are present even though the MRcollar design has two antenna rings in comparison to three rings of HYPERcollar3D. The reflector backed dipole antenna shows an excellent predicted and measured matching, i.e., $S_{11} < -20$ dB, when placed in a specifically designed dielectric encasing. Cross-coupling between two adjacent antennas is predicted to be always better than -14.9 dB, ensuring

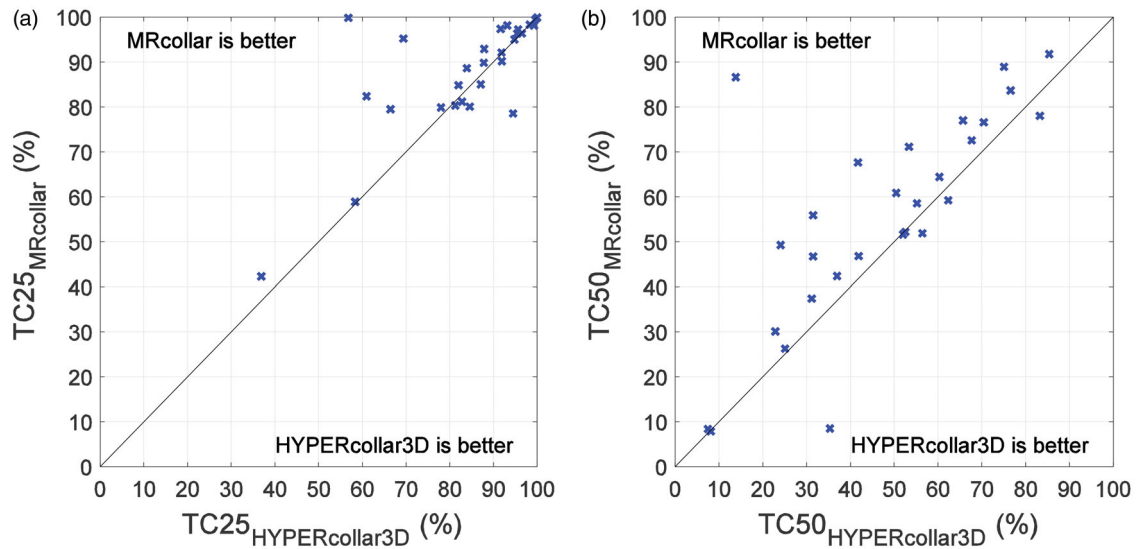


Figure 10. (a) TC25 and (b) TC50 comparisons of the MRcollar and the HYPERcollar3D models for 28 H&N patients.

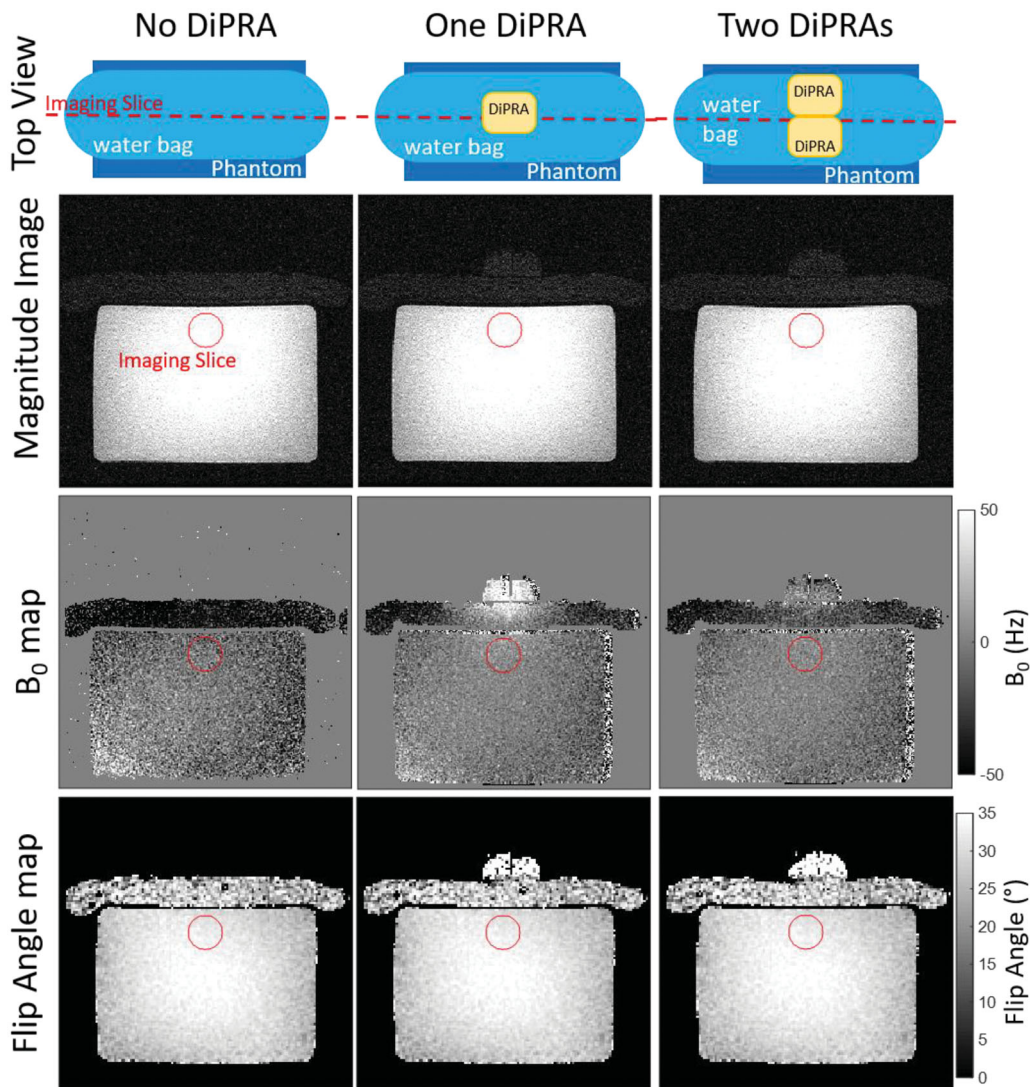


Figure 11. Results of the B₀, flip angle (mean value) and SNR measurements for the MR functionality assessment. The region of interest (ROI) is highlighted in red.

independence of the individual channels. Encasing the DiPRA also improves symmetry in the z-direction but adding the cover of the antenna encasing causes a 6 mm shift of the

maximum SAR in 10 mm depth of muscle equivalent phantom. This predicted SAR shift when adding 1 mm top cover was verified using a dedicated measurement setup. It is

caused by the y -components of the electric field that are generated since the two dipole 'arms' are on different sides of the PCB. This phenomenon is small but may impose a need to ensure a matching orientation of the antennas inside the Sim4Life model and the manufactured device. Unfortunately, the required technology to perform the ultimate experiment, i.e., microwave heating with the DiPRA modules while simultaneously measuring the temperature distribution using MR-thermometry measurements, are presently not available. We are currently in the process of implementing additional 434 MHz filtering in the MR-signal readout pathway as well as obtaining sufficient 434 MHz amplifiers to enable the final proof of functionality and future clinical hyperthermia application using the MRcollar for patients with H&N cancer. Nevertheless, the MR experiments presented here combined with those earlier reported by Sumser et al. [35] do illustrate that the DiPRA modules do not alter MR transmit/receive performance.

For the MRcollar design, we decided to replace the manually manufactured HYPERcollar3D patch antennas by reflector backed dipole antennas designed on a PCB. A downside of this antenna is that very small FDTD grid steps, i.e., 0.75 mm and 0.5 mm, are necessary to correctly resolve the thin metallic antenna parts and the antenna feeding port. This increases the computation time for each simulation approximately two times in comparison to those for the HYPERcollar3D. However, we expect that ongoing improvements in graphical processor units will allow us to complete the whole treatment planning process in around two hours, which is sufficiently fast for clinical HTP modeling. Most importantly, the antenna orientation parallel to the radiated RF pulse of the MR birdcage coil indeed ensured a limited flip angle (B_1^+) distortion within the antenna encasing.

The maximum SAR of the single reflector backed dipole antenna module inside the muscle equivalent phantom was increased by 47% when introducing the encasing around the antenna, leading to higher power delivery at the target region. This will decrease the maximum power requirements for the microwave amplifiers, which is the most expensive sub-system in RF hyperthermia systems. The antenna encasings also reduce the amount of water needed in the system by 2.5 L (31%) in comparison to the HYPERcollar3D, making it lighter and thus easier to install. The DiPRA modules also enable an independent water circulation system for the antennas from the water bolus circulation system. In this way, the temperature inside the antenna cavities can be kept constant while the temperature in the water bolus can be tailored to the superficial cooling required. When changing the water temperature by 1 °C, the resonant frequencies for the patch and waveguide antennas shift by 1.1 MHz and by 0.89 MHz respectively [33,34]. A lower water volume will also reduce water circulation-based MR distortions. In addition, the space between the DiPRA modules allows integration of an MR surface coil array close to the patient surface [35]. Such a surface coil array will increase imaging SNR and potentially enable multi-coil acceleration techniques to obtain MR thermometry maps with higher temporal resolution. With these combined approaches, the accuracy and

motion-robustness of MR thermometry in RF hyperthermia treatments is expected to improve.

Conclusion

Our results show that the novel MRcollar design enables achieving comparable heating capabilities as compared to the current clinical HYPERcollar3D. The DiPRA antenna module provides excellent predictive and measured matching characteristics and also predicted cross-coupling between adjacent antennas is predicted to be always better than -14.9 dB. The MRcollar design also reduces the amount of water needed by 31% (2.5 L), which will reduce applicator weight and water circulation-based MR distortion. The flip angle map distortions caused by the DiPRA module are found to be restricted to within the module itself. The H&N hyperthermia delivery quality with the MRcollar can be maintained, while facilitating simultaneous noninvasive MR thermometry for treatment monitoring and control.

Acknowledgment

Further authors would like to acknowledge T.V. Feddersen for proofreading and grammar check.

Disclosure statement

G. C. van Rhoon and M. M. Paulides have financial interest in Sensius BV. D. T. Yeo is an employee of GE Global Research Center.

Funding

This work was developed within the framework of COST Action MyWAVE CA17115 and it was supported by the Dutch Cancer Society under grants EMCR 2012-5472 plus 11368 and by the Ministry of Education, Youth and Sports of the Czech Republic grant LTC19031.

ORCID

Tomas Drizdal  <http://orcid.org/0000-0001-9061-8231>
 Kemal Sumser  <http://orcid.org/0000-0002-6695-2659>
 Gennaro G. Bellizzi  <http://orcid.org/0000-0003-2866-2973>
 Ondrej Fiser  <http://orcid.org/0000-0001-8259-0611>
 Jan Vrba  <http://orcid.org/0000-0001-6528-0187>
 Gerard C. van Rhoon  <http://orcid.org/0000-0002-7365-5783>
 Desmond T. B. Yeo  <http://orcid.org/0000-0002-7669-274X>
 Margarethus M. Paulides  <http://orcid.org/0000-0002-5891-2139>

References

- [1] Cihoric N, Tsikkinis A, van Rhoon G, et al. Hyperthermia-related clinical trials on cancer treatment within the ClinicalTrials.gov registry. *Int J Hyperthermia*. 2015;31(6):609-614.
- [2] Datta NR, Ordóñez SG, Gaipal US, et al. Local hyperthermia combined with radiotherapy and/or chemotherapy: recent advances and promises for the future. *Cancer Treat Rev*. 2015;41(9):742-753.
- [3] Franckena M, Stalpers LJA, Koper PCM, et al. Long-term improvement in treatment outcome after radiotherapy and hyperthermia in locoregionally advanced cervix cancer: an update of the Dutch

- Deep Hyperthermia Trial. *Int J Radiat Oncol Biol Phys.* 2008;70(4): 1176–1182.
- [4] Issels R, Kampmann E, Kanaar R, et al. Hallmarks of hyperthermia in driving the future of clinical hyperthermia as targeted therapy: translation into clinical application. *Int J Hyperthermia.* 2016; 32(1):89–95.
- [5] Togni P, Rijnen Z, Numan WCM, et al. Electromagnetic redesign of the HYPERcollar applicator: toward improved deep local head-and-neck hyperthermia. *Phys Med Biol.* 2013;58(17):5997–6009.
- [6] Rijnen Z, Togni P, Roskam R, et al. Quality and comfort in head and neck hyperthermia: a redesign according to clinical experience and simulation studies. *Int J Hyperthermia.* 2015;31(8): 823–828.
- [7] Verduijn GM, de Wee EM, Rijnen Z, et al. Deep hyperthermia with the HYPERcollar system combined with irradiation for advanced head and neck carcinoma - a feasibility study. *Int J Hyperthermia.* 2018;34(7):994–1001.
- [8] Wust P, Cho CH, Hildebrandt B, et al. Thermal monitoring: invasive, minimal-invasive and non-invasive approaches. *Int J Hyperthermia.* 2006;22(3):255–262.
- [9] Adibzadeh F, Sumser K, Curto S, et al. Systematic review of pre-clinical and clinical devices for magnetic resonance-guided radiofrequency hyperthermia. *Int J Hyperthermia.* 2020;37(1):15–27.
- [10] Paulides MM, Bakker JF, Hofstetter LW, et al. Laboratory prototype for experimental validation of MR-guided radiofrequency head and neck hyperthermia. *Phys Med Biol.* 2014;59(9): 2139–2154.
- [11] Numan WCM, Hofstetter LW, Kotek G, et al. Exploration of MR-guided head and neck hyperthermia by phantom testing of a modified prototype applicator for use with proton resonance frequency shift thermometry. *Int J Hyperthermia.* 2014;30(3): 184–191.
- [12] Tarasek MR, Pellicer R, Hofstetter LW, et al. Validation of MR thermometry: method for temperature probe sensor registration accuracy in head and neck phantoms. *Int J Hyperthermia.* 2014; 30(2):142–149.
- [13] Paulides MM, Mestrom RMC, Salim G, Adela BB, et al. A printed Yagi-Uda antenna for application in magnetic resonance thermometry guided microwave hyperthermia applicators. *Phys Med Biol.* 2017;62(5):1831–1847.
- [14] Takook P, Persson M, Gellermann J, et al. Compact self-grounded Bow-Tie antenna design for an UWB phased-array hyperthermia applicator. *Int J Hyperthermia.* 2017;33(4):387–314.
- [15] Takook P, Persson M, Trefna HD. Performance evaluation of hyperthermia applicators to heat deep-seated brain tumors. *IEEE J Electromagn RF Microw Med Biol.* 2018;2(1):18–24.
- [16] Gellermann J, Hildebrandt B, Issels R, et al. Noninvasive magnetic resonance thermography of soft tissue sarcomas during regional hyperthermia: correlation with response and direct thermometry. *Cancer.* 2006;107(6):1373–1382.
- [17] Mulder HT, Curto S, Paulides MM, et al. Systematic quality assurance of the BSD2000-3D MR-compatible hyperthermia applicator performance using MR temperature imaging. *Int J Hyperthermia.* 2018;35(1):305–313.
- [18] Yang X, Wu J, Chu X, et al. Characterization of a MRI-RF hyperthermia dual-unction coil element design. In: 19th Annual Meeting of International Society for Magnetic Resonance in Medicine, Montreal, Quebec, Canada; 2011.
- [19] Yeo DTB, Yang X, Wu J, et al. Investigation of a dual-function applicator for RF hyperthermia & MRI. In: 19th Annual Meeting of International Society for Magnetic Resonance in Medicine, Montreal, Quebec, Canada; 2011.
- [20] Winter L, Oezerdem C, Hoffmann W, et al. Thermal magnetic resonance: physics considerations and electromagnetic field simulations up to 23.5 Tesla (1GHz). *Radiat Oncol.* 2015;10:201.
- [21] Winter L, Oberacker E, Paul K, et al. Magnetic resonance thermometry: methodology, pitfalls and practical solutions. *Int J Hyperthermia.* 2016;32(1):63–75.
- [22] Paulides MM, Vossen SHJA, Zwamborn APM, et al. Theoretical investigation into the feasibility to deposit RF energy centrally in the head-and-neck region. *Int J Radiat Oncol Biol Phys.* 2005; 63(2):634–642.
- [23] Paulides MM, Stauffer PR, Neufeld E, et al. Simulation techniques in hyperthermia treatment planning. *Int J Hyperthermia.* 2013; 29(4):346–357.
- [24] Dobsicek Trefna H, Crezee J, Schmidt M, et al. Quality assurance guidelines for superficial hyperthermia clinical trials : II. Technical requirements for heating devices. *Strahlenther Onkol.* 2017; 193(5):351–366.
- [25] Verhaart RF, Fortunati V, Verduijn GM, et al. CT-based patient modeling for head and neck hyperthermia treatment planning: manual versus automatic normal-tissue-segmentation. *Radiother Oncol.* 2014;111(1):158–163.
- [26] Hasgall PA, Gennaro FD, Baumgartner C, et al. ITIS Database for thermal and electromagnetic parameters of biological tissues; 2018. Available from: www.itis.ethz.ch/database.
- [27] Rijnen Z, Bakker JF, Canters RAM, et al. Clinical integration of software tool VEDO for adaptive and quantitative application of phased array hyperthermia in the head and neck. *Int J Hyperthermia.* 2013;29(3):181–193.
- [28] Cappiello G, Drizdal T, McGinley B, et al. The potential of time-multiplexed steering in phased array microwave hyperthermia for head and neck cancer treatment. *Phys Med Biol.* 2018;63(13).
- [29] Chen S. Particle Swarm Optimization Toolbox version 20130702; 2016. Available from: <http://www.mathworks.com/matlabcentral/fileexchange/25986>.
- [30] Hoffmann J, Henning A, Giapitzakis IA, et al. Safety testing and operational procedures for self-developed radiofrequency coils. *NMR Biomed.* 2016;29(9):1131–1144.
- [31] Jezzard P, Balaban RS. Correction for geometric distortion in echo planar images from B0 field variations. *Magn Reson Med.* 1995; 34(1):65–73.
- [32] Sacolick LI, Wiesinger F, Hancu I, et al. B1 mapping by Bloch-Siegert shift. *Magn Reson Med.* 2010;63(5):1315–1322.
- [33] Paulides MM, Bakker JF, Chavannes N, et al. A patch antenna design for application in a phased-array head and neck hyperthermia applicator. *IEEE Trans Biomed Eng.* 2007;54(11): 2057–2063.
- [34] Drizdal T, Paulides M, Vrba J, et al. Waveguide-based applicators for superficial hyperthermia treatment: is tuning really required? *J Electromagn Waves Appl.* 2013;27(6):682–690.
- [35] Sumser K, Bellizzi GG, Forner R, et al. Dual-function MR-guided hyperthermia: an innovative integrated approach and experimental demonstration of proof of principle. *IEEE Trans Bio-Med Eng.* 2021;68(2):712–717.